J Mater Sci: Mater Med (2010) 21:1611–1620
DOI 10.1007/s10856-010-4028-2

Alginate-crosslinked chitosan scaffolds as pentoxifylline delivery carriers

Hsin-Yi Lin · Chih-Tsung Yeh

Received: 17 September 2009 / Accepted: 8 February 2010 / Published online: 27 February 2010

Abstract To prevent fibrous encapsulation of implants, measures are taken to suppress inflammatory reactions around them. Sustained anti-inflammatory drug release from the scaffolds can potentially be a way to reduce inflammation around these implants. Alginate-crosslinked chitosan is often used to make biocompatible tissue engineered scaffolds. However, there is a lack of quantitative studies on the drug delivery properties of alginate-crosslinked chitosan scaffolds. For this study, chitosan, crosslinked with different concentrations of alginate, was made into porous scaffolds. Infrared and thermal gravimetric analyses showed polyelectrolyte complex formation between chitosan and alginate units. The alginate-crosslinked chitosan scaffolds were more hydrophilic, showed less swelling, had lower pentoxifylline (PTX) release efficacies, were more favorable for initial cell attachment, and were mechanically stronger and more resistant to enzymatic degradation when compared to non-crosslinked chitosan scaffolds. The differences became more significant as the concentrations of chitosan and alginate increased. Furthermore, in vitro tests showed that when PTX was slowly released from the scaffolds, it became more effective in suppressing the production of TNF-α and IL-6 by stimulated macrophage cells.

H.-Y. Lin (✉) · C.-T. Yeh
Department of Chemical Engineering and Biotechnology, National Taipei University of Technology, No. 1, Sec 3, Zhongxiao E. Rd, 106 Taipei, Taiwan
e-mail: hbrunken@ntut.edu.tw; hsin_yi_lin@yahoo.com

C.-T. Yeh
e-mail: t6738039@ntut.edu.tw

H.-Y. Lin
Institute of Biotechnology, National Taipei University of Technology, No. 1, Sec 3, Zhongxiao E. Rd, 106 Taipei, Taiwan

1 Introduction

There has been an increasing interest in making biocompatible tissue engineered scaffolds with the capability to release drugs that promote successful tissue repair [1–5]. Inflammation often arises from the insertion of foreign objects like implants into the body. This can cause fibrous/collagenous encapsulation of the implants, which is the major cause for implant failures [6, 7]. Anti-inflammatory medicines have been added to biopolymeric scaffolds to be released after surgical procedures for the purpose of suppressing inflammation caused by implant insertion [8–12]. It is believed that by suppressing inflammatory reactions after the insertion of an implant, the success rate of implant surgeries improves [13].

Pentoxifylline (PTX) is an anti-inflammatory drug that is known to prevent immune cells from producing inflammatory cytokines such as IL-1, IL-6 and TNF-α [14–16] and to treat or prevent tissue fibrosis [17–19]. PTX was reported to be able to inhibit phosphodiesterase, resulting in an increase in the intracellular levels of cAMP and a decrease in inflammatory cytokine production [14, 15]. At a dosage of 100 μg/mL, PTX can suppress immune cell proliferation [16, 20]. Therefore, PTX was used as a model drug in this test.

Porous tissue-engineered scaffolds made of chitosan-alginate polyelectrolyte complex have been reported with better biocompatibility [21–23] and drug release properties [24–28] than chitosan or alginate alone. Alginate is a brown seaweed extract that is regarded as safe by the FDA [29] and has been shown to have little or no immune reactions in the nearby tissue [30, 31]. In vitro and in vivo results have shown that alginate is osteogenic [21–23, 26]. Chitosan is a natural polymer that has been studied as a material for sustained drug release [32–34] and for tissue

engineered scaffolds [35, 36]. It is readily available, biocompatible, and bioresorbable. Alginate is often chemically crosslinked with chitosan to modify its abilities to uptake and release medicines [22–28].

Compounds such as anti-inflammatory and anti-bacterial drugs and growth factors have been added to implantable scaffolds to improve tissue repair [2–5, 8, 12, 37]. However, their effects on cellular and tissue reactions were often evaluated *qualitatively*. The strength and concentrations of these compounds affect the consistency of their performance in vivo, which may lead to adverse side effects [38]. It is important to *quantitatively* characterize the scaffolds' drug release properties and how changes in these properties affect subsequent biological reactions.

In this study, chitosan and alginate-crosslinked chitosan porous scaffolds were tested as drug carriers. The effects that various degrees of crosslinking had on the pore structures, degradation rates, mechanical strengths, cell attachments, swelling ratios, and the PTX release efficacies of chitosan scaffolds were investigated. At the same time, the effects of PTXs release rates on its effectiveness in reducing inflammatory cytokine production by macrophage cells was also studied.

2 Materials and methods

All chemicals used in this study were purchased from Sigma, MO, USA, unless specified otherwise.

2.1 Preparation of chitosan and alginate-crosslinked chitosan solutions

Chitosan (96% deacetylation, C&B Co., Taiwan) was dissolved in a 2 v/v% acetic acid solution. Sodium alginate (Acros Organics, NJ, USA) was dissolved in deionized (DI) water. Chitosan and alginate solutions were stirred together for an hour before they were further processed into films and scaffolds. Five solutions were made. The final concentrations of the two polymers were 1% chitosan and no alginate (C1), 1% chitosan and 0.5% alginate (C1A0.5), 1% chitosan and 1% alginate (C1A1), 1% chitosan and 2% alginate (C1A2) and 2% chitosan and 1% alginate (C2A1). Films and porous scaffolds made from the five polymer solutions will be denoted as listed above. Films were used for contact angle and cell attachment tests and scaffolds were used for all other tests.

2.2 Making films and scaffolds

One milliliter of a polymer solution was coated on the bottom of each polystyrene petri dish ($D = 3$ cm) and air dried at room temperature. Two milliliters of polymer solutions were poured into glass tubes and then frozen at −20°C overnight. The frozen samples were then lyophilized in a freeze dryer (RVT4104, Savant, NY, USA). Films and lyophilized scaffolds were neutralized in 0.5 N NaOH for 30 min, rinsed with DI water three times, dehydrated using a series of ethanol solutions (20, 50, 70 and 100%) and air dried.

2.3 Thermo-gravimetric analysis (TGA) ($n = 4$)

Dried scaffolds were cut into small pieces (~10 mg) and put into a TGA instrument (Thermal analyst 2000, TA Instruments, USA). The TGA instrument's sample chamber was flushed with nitrogen gas before and during the test (60 mL/min). Scaffolds were heated from 25 to 600°C at 10°C/min and their weights were recorded over time. The percentage of derivative weight loss was plotted verses temperature to find the decomposition temperature.

2.4 Fourier transform infrared spectrum (FTIR) ($n = 3$)

Scaffold specimens were ground, mixed with KBr, and pressed into tabs. They were then scanned from 4,000 to 400 cm^{-1} in a FTIR machine (Spectrum Gx, PerkinElmer, MA, USA) with a resolution of 4 cm^{-1}. Transmittance peaks were identified.

2.5 Contact angle ($n = 4$)

Five microliters of DI water were placed on each polymer film. Static contact angles were measured using a contact angle meter (CA-D, Kyowa Interface Science Co., Japan).

2.6 Scaffold morphology by scanning electron microscope (SEM) ($n = 3$)

Dried scaffolds were sliced and sputter coated with gold before being placed in the vacuum chamber of a SEM (Hitachi S-3000H, Japan). Microphotographs of the scaffold surfaces were taken.

2.7 Swelling ratio ($n = 3$)

After measuring the diameters (D_o) of each dry scaffold ($D \sim 1$ cm, $h \sim 0.2$ cm), they were placed in phosphate buffered saline (PBS, pH = 7.4) and their diameters were measured at each designated time point (D_t). The swelling ratio at each time point was calculated as $[(D_t - D_o)/D_o] \times 100\%$.

2.8 Release efficiency of pentoxifylline (PTX) ($n = 3$)

Each dry scaffold disc ($D \sim 1$ cm, $h \sim 0.2$ cm) was loaded with 100 μL PTX (20 mg/mL) and left to dry at room temperature overnight. Ten scaffold discs were placed in a beaker filled with 100 mL of PBS, three beakers ($n = 3$) for each polymer. All beakers were placed on a shaker (50 rpm) during the test. At each designated time point, 100 μL of PBS was sampled and the same volume of PBS was then replenished. The absorbance of PTX at 274 nm was measured (Gene Quant 1300 spectrophotometer, GE Healthcare, NJ) and converted to concentrations (M_t (μg/mL)) using a standard curve. The release efficiency of the PTX was calculated as $[(M_t/200\ \mu g/mL)] \times 100\%$. After the PTX in the ten scaffolds was released, the final PTX concentration in each beaker was 200 μg/mL.

2.9 Degradation ($n = 3$)

The chitosan used to make samples for the degradation test was 82% deacetylated because it is more easily degraded by lysozyme than 96% deacetylated chitosan [39]. A scaffold with an initial dry weight of W_o was placed in a 15 mL centrifuge tube filled with 5 mL of lysozyme solution (70,000 U/mL PBS, pH = 7.4). The tubes were placed in an incubator (37°C) and the lysozyme solution was changed every 3 days. On days 7, 14 and 21, three tubes of each specimen were removed from the incubator, and the remaining scaffolds were rinsed carefully several times with DI water and air dried to obtain their dry weights (W). The percentage of weight loss was calculated as $[(W_o - W)/W_o] \times 100\%$.

2.10 Compression ($n = 4$)

Dry scaffolds ($D \sim 1$ cm, $h \sim 1.2$ cm) were submerged in PBS overnight and excess liquid was removed before testing. A Universal Micro-tribometer (model UMT-2, CETR, CA, USA) was used to obtain stress–strain curves. The exact diameter and height of each scaffold was measured right before the test. A 10 N load cell was used and the speed of the crosshead was set at 0.3 mm/s. The test ended when the crosshead reached 80% strain of the scaffold. The slope of the initial linear section of the stress–strain curve was used to estimate the Young's modulus.

2.11 Cell attachment ($n = 4$)

The bottom of each well of a 24-well tissue culture polystyrene (TCP) plate (BD Biosciences, CA) was coated with 200 μL of polymer solution and air dried. The TCP surface served as positive control. Films were processed as described earlier. Coated films were disinfected with 70% ethanol solution, exposed to UV briefly, and then rinsed with sterile PBS to remove residual ethanol. Osteoblasts (7F2, ATCC, VA) (3×10^5 cells/mL) were seeded onto the films (1 mL/well). Cells were cultured in α-MEM (Invitrogen, CA, USA) without serum. The culture was maintained in a cell culture incubator (SCA-165DS, ASTEC, Japan) at 95% humidity, 37°C, and 5% CO_2. At designated time points, unattached cells were counted to back calculate the number of attached cells.

2.12 In vitro test of anti-inflammatory effect during controlled release ($n = 4$)

The test was done using C1 and C1A2 scaffolds to compare the effects caused by varying degrees of slow release. Scaffolds were each loaded with 50 μL of PTX (4 mg/mL) and allowed to dry at room temperature. Macrophage cells (RAW 264.7, ATCC, VA) were seeded into 24-well TCP plates at $1 \times 10^5/cm^2$ and allowed to settle overnight in a cell culture incubator. Cell culture media (DMEM plus 10% fetal bovine serum, 100 U/mL penicillin, 100 μg/mL streptomycin) was then removed, and the cells were separated into four different test groups—(1) DMEM: cells cultured in DMEM with a blank scaffold, (2) DMEM + LPS: cells in DMEM + 1 μg/mL LPS + blank scaffold, (3) DMEM + LPS + PTX (in media): cells in DMEM + 1 μg/mL LPS + 100 μg/mL PTX + blank scaffold, and (4) DMEM + LPS + PTX (from scaffold): cells in DMEM + 1 μg/mL LPS + scaffold loaded with 100 μg PTX [16]. Each well contained 2 mL of medium.

Lipopolysaccharide (LPS, 1 μg/mL) was used to activate the macrophage cells to release inflammatory factors [40]. Six hours later, tumor necrosis factor alpha (TNF-α) and interleukin 6 (IL-6) in the media were measured using commercial kits (Mouse TNF-alpha ELISA OptiEIA, BD Bioscience, CA, and Mouse IL-6 ELISA DuoSet, R&D, MN).

2.13 Statistical analysis

All data is presented as average ± standard deviation. Statistical analysis was conducted using two-way ANOVA with Tukey tests (SigmaStat 3.5 for Windows, Systat Software, IL). Difference between alginate-crosslinked chitosan and chitosan was declared when $P < 0.05$.

3 Results and discussion

3.1 TGA and FT-IR

Both TGA and FTIR were used to characterize bond formation between chitosan and alginate. The decomposition

temperatures of all polymer samples are listed in Table 1. Compared to chitosan (306°C), the decomposition temperatures of alginate-crosslinked chitosan decreased as the concentrations of alginate increased ($P < 0.05$). The increase in chitosan concentration had no significant effect on the temperature since C2A1 had a similar decomposition temperature as C1A1 ($P > 0.05$). The decomposition temperature of pure alginate was 251.3°C. The decomposition temperatures of alginate-crosslinked chitosan fell between those of chitosan and alginate, indicating that covalent bond formation did not take place [41, 42]. Alginate, an anionic polysaccharide, will form polyelectrolyte complex with chitosan, a cationic polysaccharide, through ionic attraction between the NH_3^+ of chitosan and the COO^- of alginate [22, 23, 43].

The carboxylate vibration bands of alginate are typically at 1,412 cm^{-1} (symmetric) and 1,596 cm^{-1} (asymmetric vibration) [44]. Chitosan's amine group has typical absorbance at 1,587 and 1,647 cm^{-1} (amide I). The 1,587 cm^{-1} peak is assigned to the N–H bending vibration of amine overlapping amide II vibration [44]. After chitosan was crosslinked with alginate, three new peaks emerged at 1407, 1554, and 1616 cm^{-1} (Fig. 1). The XPS analysis from Lawrie et al. [44] showed that the 1,616 cm^{-1} peak was due to amide I and asymmetric NH_3^+ deformation. Peak at 1,554 cm^{-1} was assigned to amide II (9%) overlapping amine (36%) and protonated amine (55%). The intensity of the peak at 1,554 cm^{-1} decreased as the amount of alginate increased. The peak at 1,407 cm^{-1} was assigned to the alginate's carboxylate vibration.

3.2 Contact angle

The contact angles (Table 1) of alginate-crosslinked chitosan were all smaller than that of chitosan ($P < 0.05$ except for C2A1). As the ratio of alginate increased, the contact angles of crosslinked chitosan got smaller. C2A1 had a higher contact angle compared to that of C1A1 ($P < 0.05$).

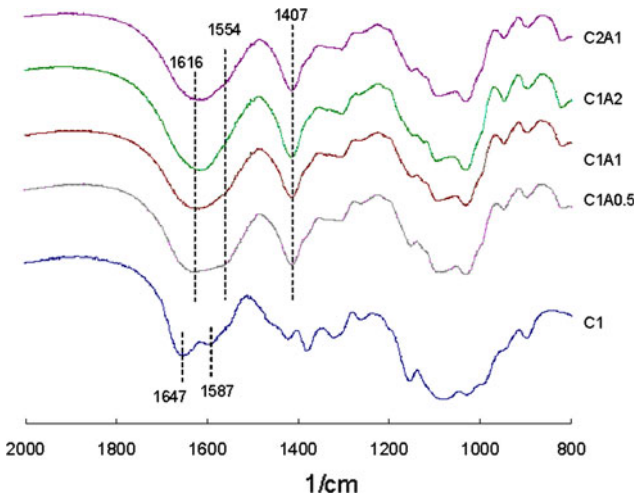

Fig. 1 Fourier transform infrared (FTIR) spectra of chitosan and alginate-crosslinked chitosan scaffolds

Alginate is water soluble and more hydrophilic than chitosan. As the concentration of chitosan increases in the chitosan-alginate complex, the hydrophilicity decreases. On the other hand, as the percentage of alginate increases in the complex, its hydrophilicity increases.

3.3 SEM

As more alginate was added to chitosan, the pores of the chitosan scaffolds became more closed (less interconnectivity) and smaller. The texture of the scaffold walls became flaky as the percentage of alginate increased (Fig. 2). Increasing chitosan concentration (Fig. 2e) resulted in more honeycomb-like pores and a less flaky texture.

Chung et al. [23] reported decreased porosity and pore size after chitosan was crosslinked with alginate. The scaffolds had fewer pores and a more closed structure. Polyelectrolyte complex and ionic bonds between the two polymers were thought to result in a less porous structure [23, 45].

Table 1 Decomposition temperatures, contact angles, swelling ratios and Young's moduli of chitosan and alginate-crosslinked-chitosan films and scaffolds

	1. Decomposition temperature (°C)*	2. Contact angle (°)	3. Swelling ratio at 90 min (%)	4. Young's modulus (kPa)
C1	306.3 ± 0.3^a	82.8 ± 3.1^a	34.3 ± 1.1^a	2.3 ± 0.2^a
C1A0.5	299.5 ± 0.7^b	69.0 ± 2.9^b	32.8 ± 0.2^b	3.1 ± 0.0^b
C1A1	269.4 ± 0.7^c	55.5 ± 2.6^c	29.5 ± 0.1^c	3.5 ± 0.4^c
C1A2	266.4 ± 0.7^d	48.0 ± 1.6^d	27.8 ± 0.2^d	6.8 ± 0.0^d
C2A1	298.1 ± 1.5^b	77.0 ± 2.4^a	23.9 ± 0.1^e	9.6 ± 0.9^e

Data represent the mean ± standard deviation ($n = 4$, two-way ANOVA). Numbers marked with different letters are statistically different (only for numbers within the same column)

* The onset decomposition temperature of pure alginate is 251.3 ± 1.4°C

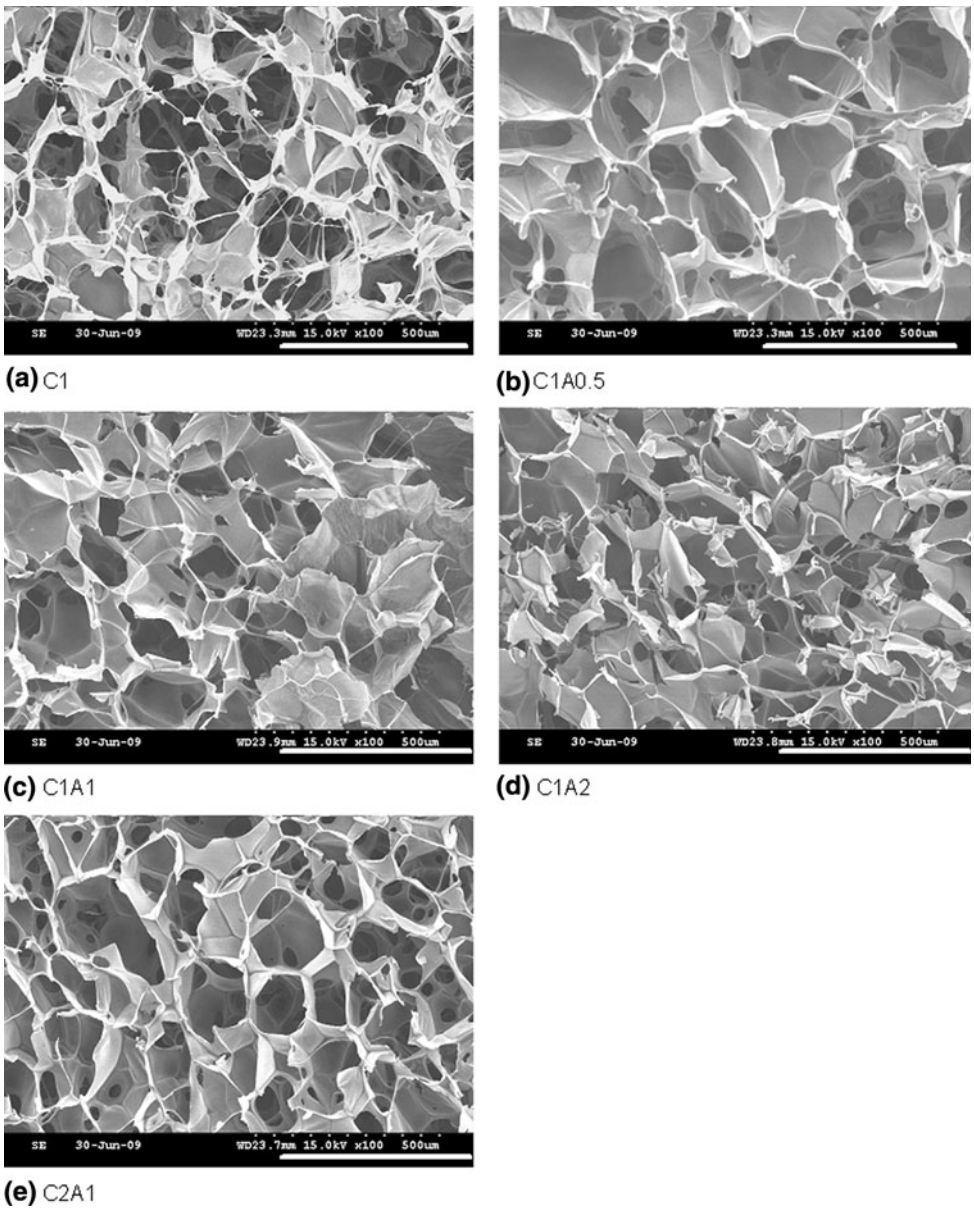

Fig. 2 Representative SEM microphotographs of **a** C1 (1% chitosan), **b** C1A0.5 (1% chitosan + 0.5% alginate), **c** C1A1 (1% chitosan + 1% alginate), **d** C1A2 (1% chitosan + 2% alginate), **e** C2A1 (2% chitosan + 1% alginate) scaffolds. Scale bar = 500 μm for all micrographs

3.4 Swelling ratio

Figure 3 shows the swelling ratios of the scaffolds during the first 60 min of the test. The swelling ratios of the scaffolds after 90 min in PBS are listed in Table 1. Scaffolds crosslinked with alginate swelled up more slowly than uncrosslinked chitosan scaffolds. The higher the alginate concentration was, the slower the scaffold swelled. The swelling ratios of alginate-crosslinked scaffolds were significantly smaller than those made of uncrosslinked chitosan ($P < 0.05$). Increased concentrations of chitosan also reduced the scaffold's swelling ratio ($P < 0.0.5$).

The chains of the two polymers formed a branched network through electrostatic attraction between the two oppositely charged polymer chains. The branched network prevents polymer chains from stretching and swelling freely [22]. Without the ionic bonding, scaffolds with higher polymer mass would have swelled more at the end of the test. Compared with C1A1, the increase in chitosan percentage in C2A1 made its scaffolds more hydrophobic and had smaller pores. As a result, the C2A1 scaffolds swelled less than the C1A1 scaffolds.

3.5 Release efficiency

By 90 min, C1, C1A0.5, C1A1, C1A2, and C2A1 scaffolds released 93.4, 85.7, 83.1, 78.6, and 70.7% of their total PTX respectively (Fig. 4). As the percentages of alginate in the scaffolds increased, the scaffolds' release efficiencies

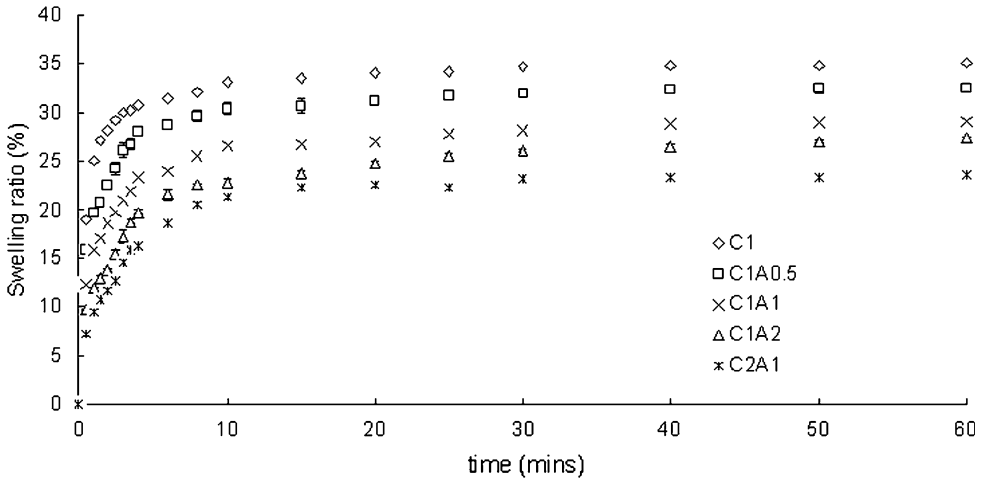

Fig. 3 The swelling ratios of chitosan and alginate-crosslinked chitosan scaffolds

decreased. C2A1 had the lowest release efficacy and lowest initial PTX burst of all samples.

The scaffolds made from solutions with higher polymer concentrations had higher polymer densities, which resulted in lower mass transportation inside the scaffolds. Vandenberg et al. [27] observed lower protein release efficiency in alginate microcapsules coated with higher concentrations of chitosan. Between groups with similar polymer mass (C2A1 and C1A2), C2A1 released less PTX over time. Besides having a smaller swelling ratio, C2A1 was more hydrophobic and had smaller pores, which slowed down aqueous-phase mass transfer. Chitosan microspheres crosslinked with alginate were shown to have less release capability for lipophilic drugs [24].

3.6 Degradation

The addition of alginate significantly reduced the percentage of degradation in the chitosan scaffolds compared to the uncrosslinked chitosan scaffolds (Fig. 5). Takeuchi et al. [28] observed a lower eroding rate in chitosan-alginate composite particles than in alginate particles. Between scaffolds with similar polymer mass, i.e. C1A1 and C1A2, their percentages of degradation were similar throughout the test. The percentages of degradation seemed to be more dependent on polymer density than the degree of crosslinking.

Lysozyme targets and hydrolyzes glycosidic *bonds* (C–O–C) [46–48] of chitosan and alginate polymers. Ionic attraction due to crosslinking would have minimal effect on preventing lysozyme from interacting with the polymer complex.

3.7 Compression

The Young's moduli of chitosan scaffolds increased as the concentrations of alginate and chitosan increased ($P < 0.05$) (Table 1). Compared to C1, the moduli of

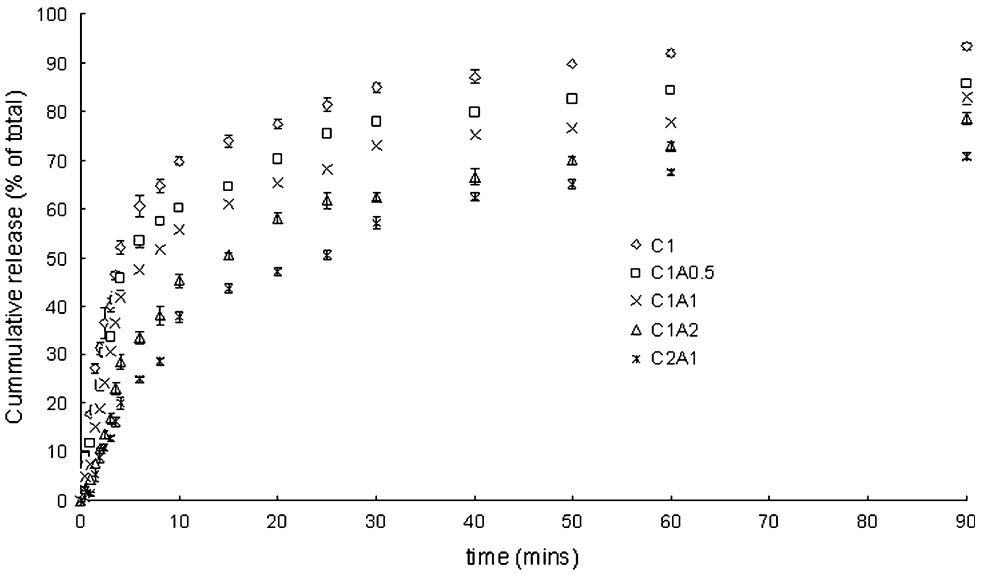

Fig. 4 The release efficacies of chitosan and alginate-crosslinked chitosan scaffolds

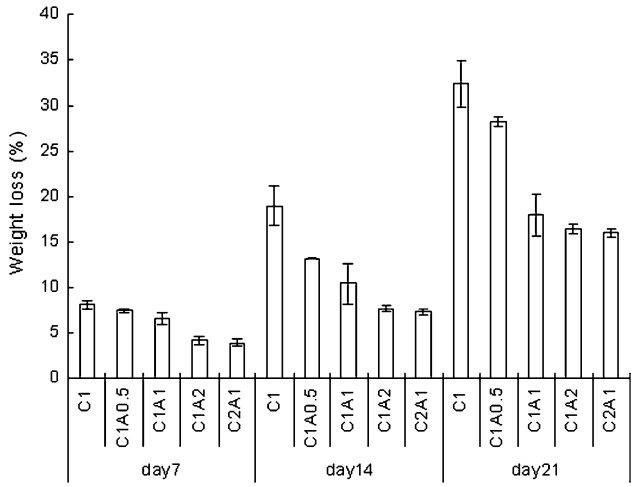

Fig. 5 The percentages of weight loss of chitosan and alginate-crosslinked chitosan scaffolds due to enzymatic degradation over time

C1A0.5 and C1A1 were not significantly higher. However, the modulus of the C1A2 scaffold was almost twice as much as that of C1A1. The higher polymer mass and smaller pores may have resulted in the higher compressional Young's moduli of the C1A2 scaffolds. With a similar amount of polymer mass, C1A2 had a lower modulus than C2A1. Hence besides polymer mass, different degrees of crosslinking could also cause differences in scaffolds' moduli.

Li et al. [22] reported chitosan and alginate-crosslinked chitosan scaffolds to have Young's moduli of 2.56 and 8.16 MPa respectively. They had used a 4.8% chitosan-alginate 1:1 mixture instead of the 2% in this test and their test was done on dry scaffolds. Nonetheless, we can see that alginate crosslinking has significantly increased the compressional moduli of chitosan scaffolds.

3.8 Cell attachment

After 1 and 1.5 h, films with higher alginate content were more favorable for cell attachment (Fig. 6). At 2 h, C2A1 had the lowest percentage of cell attachment of all ($P < 0.05$).

Most cells prefer to attach to more hydrophilic surfaces [49]. Increased cell attachment and proliferation on chitosan scaffolds after they had been crosslinked with alginate have also been seen by others [21, 22]. C2A1 and C1 had similar hydrophobicity (Table 1) and similar percentages of initial cell attachment.

3.9 Anti-inflammatory effect of PTX slow release

There was a significant difference between the release efficiencies of C1 and C1A2, hence the test was done on the two specimens. Macrophage cells did not release TNF-α and IL-6 in the presence of scaffolds (DMEM groups in Fig. 7a, b) over the first 24 h. With 1 μg/mL of LPS (DMEM + LPS), macrophage cells released similar amounts of TNF-α and IL-6 between the two groups. When PTX was present in the media containing LPS (DMEM + LPS + PTX (in media)), the amounts of TNF-α and IL-6 were slightly lower than those in the DMEM + LPS group. There was no significant difference between the two groups since PTX did not come from the scaffolds. When scaffolds were loaded with PTX, and PTX was slowly released it into media containing LPS

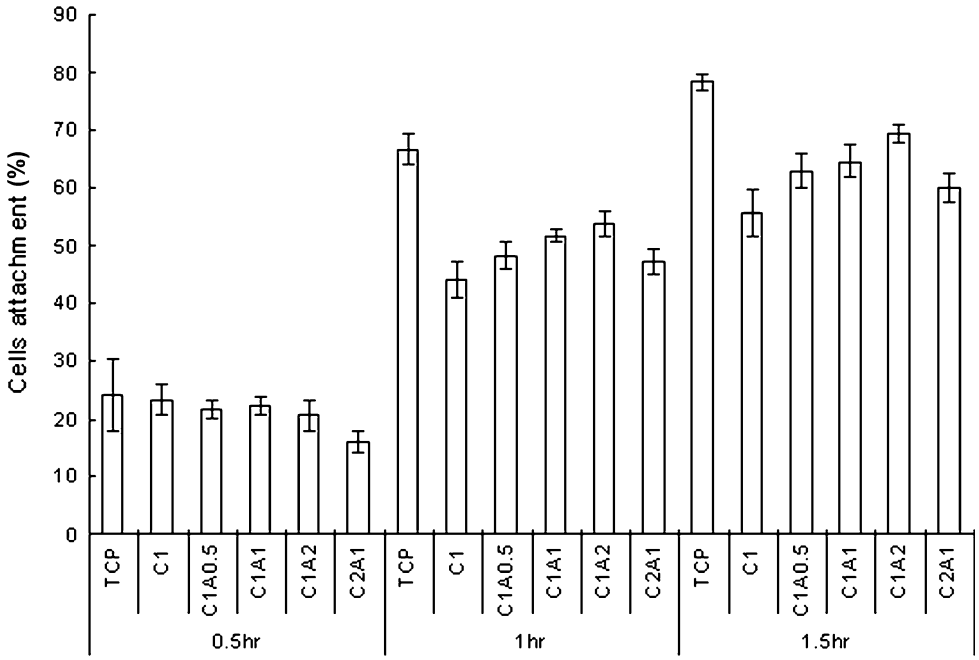

Fig. 6 Percentages of initial cell attachment on chitosan and alginate-crosslinked chitosan surfaces

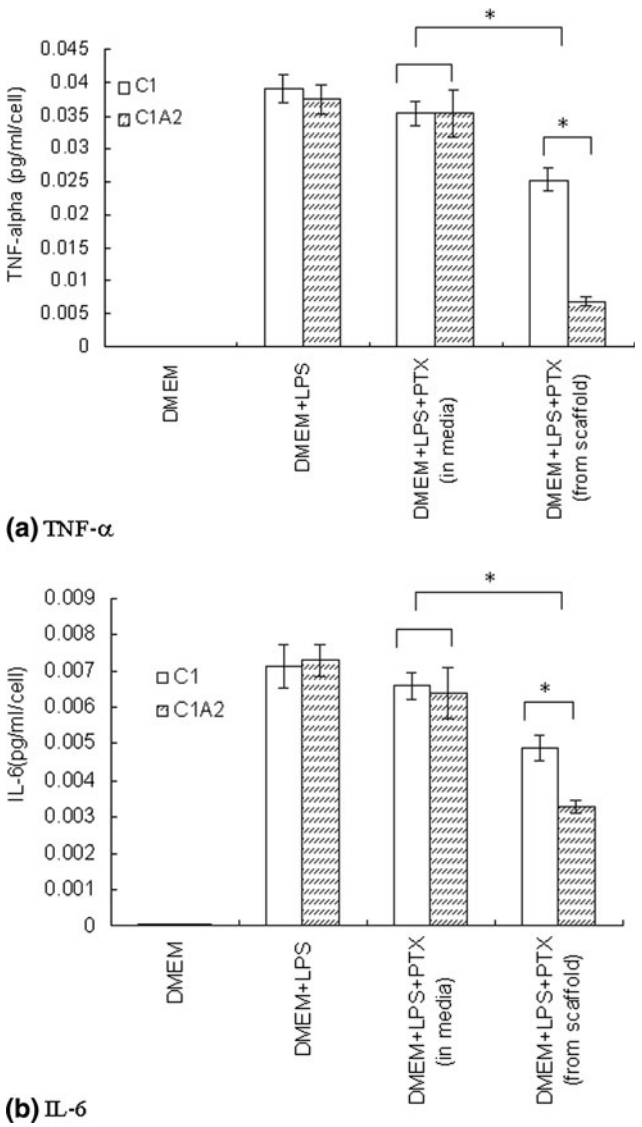

Fig. 7 Tumor necrotic factor alpha (TNF-α) (**a**) and interleukin 6 (IL-6) (**b**) release from the four conditions: DMEM: cells cultured in DMEM with a blank scaffold, DMEM + LPS: cells in DMEM + 1 μg/mL LPS + blank scaffold, DMEM + LPS + PTX (in media): cells in DMEM + 1 μg/mL LPS + 100 μg/mL PTX + blank scaffold, DMEM + LPS + PTX (from scaffold): cells in DMEM + 1 μg/mL LPS + scaffold loaded with 100 μg PTX

(DMEM + LPS + PTX (from scaffold)), the amounts of TNF-α and IL-6 were significantly lower than those in DMEM + LPS + PTX (in media) ($P < 0.05$). Furthermore, the amounts of IL-6 and TNF-α were significantly lower in C1A2 than in C1 ($P < 0.05$).

The slow release of PTX more effectively prevented macrophages from releasing pro-inflammatory factors compared to the direct delivery of PTX into the media. PTX was found to be able to decrease oxidative stress during inflammation and to suppress the superoxide production of macrophage [14, 17]. Based on the three possible cellular metabolic pathways of PTX [15], it is speculated that in this test when a high dosage of PTX was added to macrophage cells, it was used not only in suppressing TNF-α mRNA and the sequential IL-6 expressions, but also in inhibiting cell proliferation [20]. In other words, PTX was metabolized via several pathways. However, when PTX was slowly released from a scaffold, its concentration went from zero to an optimal concentration (<10 μg/mL [20]) that could suppress TNF-α expression but not cell growth or superoxide production. The slow release thus allowed for a more efficient use of PTX in macrophages in reducing the expression of TNF-α. Kofuji et al. [50] implanted chitosan beads retaining the anti-inflammatory drug prednisolone (PS) into the back of mice and investigated the therapeutic efficacy of sustained PS release against local inflammation. They found that the implantation of chitosan beads loaded with PS significantly reduced inflammation compared with the injection of PS suspension. They concluded that sustained PS release provides a minimum effective dose and facilitated prolonged periods of local drug presence. With the direct injection of PS suspension, most of the drug would be removed in the process of diffusion because of its high concentration gradient.

4 Summary

The concentration of alginate significantly changed the properties of the chitosan scaffolds measured in this test. It was hard to discern whether the changes in chitosan scaffolds' swelling ratio, release efficacy, degradation, and compressive Young's modulus were the results of alginate crosslinking or of increases in polymer mass in the scaffolds. Our results also show that a slow release of PTX can more effectively suppress inflammatory reactions in macrophage cells.

Acknowledgement This project is funded mainly by grants from the National Science Council: NSC 97-2221-E-027-001.

References

1. Langer R, Tirrell DA. Designing materials for biology and medicine. Nature. 2004;428:487–92.
2. Ho YC, Mi FL, Sung HW, Kuo PL. Heparin-functionalized chitosan-alginate scaffolds for controlled release of growth factor. Int J Pharm. 2009;376:69–75.
3. De la Riva B, Nowak C, Sánchez E, Hernández A, Schulz-Siegmund M, Pec MK, et al. VEGF-controlled release within a bone defect from alginate/chitosan/PLA-H scaffolds. Eur J Pharm Biopharm. 2009;73:50–8.
4. Holland TA, Bodde EW, Cuijpers VM, Baggett LS, Tabata Y, Mikos AG, et al. Degradable hydrogel scaffolds for in vivo delivery of single and dual growth factors in cartilage repair. Osteoarthr Cartil. 2007;15:187–97.

5. Tabata Y. Significance of release technology in tissue engineering. Drug Discov Today. 2005;10:1639–46.
6. Goreish HH, Lewis AL, Rose S, Lloyd AW. The effect of phosphorylcholine-coated materials on the inflammatory response and fibrous capsule formation: in vitro and in vivo observations. J Biomed Mater Res A. 2004;68:1–9.
7. Vicreconti M, Monti L, Muccini R, Bernakiewicz M, Toni A. Even a thin layer of soft tissue may compromise the primary stability of cementless hip stems. Clin Biomech. 2001;16:765–75.
8. Chvatal SA, Kim YT, Bratt-Leal AM, Lee H, Bellamkonda RV. Spatial distribution and acute anti-inflammatory effects of methylprednisolone after sustained local delivery to the contused spinal cord. Biomaterials. 2008;29:1967–75.
9. Nikkola L, Seppälä J, Harlin A, Ndreu A, Ashammakhi N. Electrospun multifunctional diclofenac sodium releasing nanoscaffold. J Nanosci Nanotechnol. 2006;6:3290–5.
10. Ju YM, Yu B, West L, Moussy Y, Moussy F. A dexamethasone-loaded PLGA microspheres/collagen scaffold composite for implantable glucose sensors. J Biomed Mater Res A. doi:10.1002/jbm.a.32512.
11. Prabaharan M, Rodriguez-Perez MA, de Saja JA, Mano JF. Preparation and characterization of poly(L-lactic acid)-chitosan hybrid scaffolds with drug release capability. J Biomed Mater Res B Appl Biomater. 2007;81:427–34.
12. Ma JY, Jiang WW, Zhou ZT, Li JM, Wang HY. The promoting angiogenesis and anti-inflammation effect of scutellarin on polyglycolic acid scaffold of balb/c mice model. J Asian Nat Prod Res. 2008;10:1147–53.
13. Revell PA. The combined role of wear particles, macrophages and lymphocytes in the loosening of total joint prostheses. J R Soc Interface. 2008;5:1263–78.
14. Bessler H, Gilgal R, Djaldetti M, Zahavi I. Effect of pentoxifylline on the phagocytic activity, cAMP levels, and superoxide anion production by monocytes and polymorphonuclear cells. J Leukoc Biol. 1986;40:747–54.
15. Costantini TW, Deree J, Loomis W, Putnam JG, Choi S, Baird A, et al. Phosphodiesterase inhibition attenuates alterations to the tight junction proteins occludin and ZO-1 in immunostimulated Caco-2 intestinal monolayers. Life Sci. 2009;84:18–22.
16. Bruynzeel I, Stoof TJ, Willemze R. Pentoxifylline and skin inflammation. Clin Exp Dermatol. 1998;23:168–72.
17. Pardakhti A, Alavi SA, Kheshti NM, Eshaghi P, Safaeian L. Effect of slow release pentoxifylline and captopril on delayed pulmonary complications of mustard gas in animal models. Tanaffos. 2009;8:41–9.
18. Berman B, Duncan MR. Pentoxifylline inhibits normal human dermal fibroblast in vitro proliferation, collagen, glycosaminoglycan, and fibronectin production, and increases collagenase activity. J Investig Dermatol. 1989;92:605–10.
19. Berman B, Wietzerbin J, Sanceau J, Merlin G, Duncan MR. Pentoxifylline inhibits certain constitutive and tumor necrosis factor-α induced activities of human normal dermal fibroblasts. J Investig Dermatol. 1992;98:706–12.
20. Vukanić ZS, Čolić M, Dimitrijević M. Effect of pentoxifylline on differentiation and maturation of human monocyte-derived dendritic cells in vitro. Int Immunopharmacol. 2007;7:167–74.
21. Li Z, Zhang M. Chitosan-alginate as scaffolding material for cartilage tissue engineering. J Biomed Mater Res A. 2005;75:485–93.
22. Li Z, Ramay HR, Hauch KD, Xiao D, Zhang M. Chitosan-alginate hybrid scaffolds for bone tissue engineering. Biomaterials. 2005;26:3919–28.
23. Chung TW, Yang J, Akaike T, Cho KY, Nah JW, Kim SI, et al. Preparation of alginate/galactosylated chitosan scaffold for hepatocyte attachment. Biomaterials. 2002;23:2827–34.
24. Ribeiro AJ, Neufeld RJ, Arnaud P, Chaumeil JC. Microencapsulation of lipophilic drugs in chitosan-coated alginate microspheres. Int J Pharm. 1999;187:115–23.
25. Shu XZ, Zhu KJ. The release behavior of brilliant blue from calcium-alginate gel beads coated by chitosan: the preparation method effect. Eur J Pharm Biopharm. 2002;53:193–201.
26. Olmez SS, Korkusuz P, Bilgili H, Senel S. Chitosan and alginate scaffolds for bone tissue regeneration. Pharmazie. 2007;62:423–31.
27. Vandenberg GW, Drolet C, Scott SL, de la Noüe J. Factors affecting protein release from alginate-chitosan coacervate microcapsules during production and gastric/intestinal simulation. J Control Release. 2001;77:297–307.
28. Takeuchi H, Yasuji T, Yamamoto H, Kawashima Y. Spray-dried lactose composite particles containing an ion complex of alginate-chitosan for designing a dry-coated tablet having a time-controlled releasing function. Pharm Res. 2000;17:94–9.
29. George M, Abraham TE. Polyionic hydrocolloids for the intestinal delivery of protein drugs: alginate and chitosan—a review. J Control Release. 2006;114:1–14.
30. Zimmermann U, Klöck G, Federlin K, Hannig K, Kowalski M, Bretzel RG, et al. Production of mitogen-contamination free alginates with variable ratios of mannuronic acid to guluronic acid by free flow electrophoresis. Electrophoresis. 1992;13:269–74.
31. Mumper RJ, Hoffman AS, Puolakkainen PA, Bouchard LS, Gombotz WR. Calcium-alginate beads for the oral delivery of transforming growth factor-β1 (TGF-β1): stabilization of TGF-β1 by the addition of polyacrylic acid within acid-treated beads. J Control Release. 1994;30:241–51.
32. Chandy T, Sharma CP. Chitosan matrix for oral sustained delivery of ampicillin. Biomaterials. 1993;14:939–44.
33. Illum L. Chitosan and its use as a pharmaceutical excipient. Pharm Res. 1998;15:1326–31.
34. Illum L, Jabbal-Gill I, Hinchcliffe M, Fisher AN, Davis SS. Chitosan as a novel nasal delivery system for vaccines. Adv Drug Deliv Rev. 2001;51:81–96.
35. Machado CB, Ventura JM, Lemos AF, Ferreira JM, Leite MF, Goes AM. 3D chitosan–gelatin–chondroitin porous scaffold improves osteogenic differentiation of mesenchymal stem cells. Biomed Mater. 2007;2:124–31.
36. Richardson SM, Hughes M, Hunt JA, Freemont AJ, Hoyland JA. Human mesenchymal stem cell differentiation to NP-like cells in chitosan-glycerophosphate hydrogels. Biomaterials. 2008;29:85–93.
37. Hou LT, Liu CM, Liu BY, Chang PC, Chen MH, Ho MH, et al. Tissue engineering bone formation in novel recombinant human bone morphogenic protein 2-atelocollagen composite scaffolds. J Periodontol. 2007;78:335–43.
38. Kerbel RS. Growth factors as mediators of malignant tumor progression. Cancer Metastasis Rev. 1993;12:215–7.
39. Aiba S. Studies on chitosan: 4. Lysozymic hydrolysis of partially *N*-acetylated chitosans. Int J Biol Macromol. 1992;14:225–8.
40. Lin H, Bumgardner JD. In vitro biocorrosion of Co–Cr–Mo implant alloy by macrophage cells. J Orthop Res. 2004;22:1231–6.
41. Ribeiro AJ, Silva C, Ferreira D, Veiga F. Chitosan-reinforced alginate microspheres obtained through the emulsification/internal gelation technique. Eur J Pharm Sci. 2005;25:31–40.
42. Wendlandt WW. Thermal analysis. 3rd ed. New York: Wiley; 1986.
43. Takahashi T, Takayama K, Machida Y, Nagai T. Characteristics of polyion complexes of chitosan with sodium alginate and sodium polyacrylate. Int J Pharm. 1990;61:35–41.
44. Lawrie G, Keen I, Drew B, Chandler-Temple A, Rintoul L, Fredericks P, et al. Interactions between alginate and chitosan

biopolymers characterized using FTIR and XPS. Biomacromolecules. 2007;8:2533–41.
45. Madihally SV, Matthew HW. Porous chitosan scaffolds for tissue engineering. Biomaterials. 1999;20:1133–42.
46. Höltje JV. Lysozyme substrates. EXS. 1996;75:105–10.
47. Kuroki R, Ito Y, Kato Y, Imoto T. A covalent enzyme-substrate adduct in a mutant hen egg white lysozyme (D52E). J Biol Chem. 1997;272:19976–81.
48. Kirby AJ. The lysozyme mechanism sorted—after 50 years. Nat Struct Biol. 2001;8:737–9.
49. Hamdan M, Blanco L, Khraisat A, Tresguerres IF. Influence of titanium surface charge on fibroblast adhesion. Clin Implant Dent Relat Res. 2006;8:32–8.
50. Kofuji K, Akamine H, Qian CJ, Watanabe K, Togan Y, Nishimura M, et al. Therapeutic efficacy of sustained drug release from chitosan gel on local inflammation. Int J Pharm. 2004; 272:65–78.